Experimental and numerical study of heat transfer across insulation wall of a refrigerated integral panel van

Patrick Glouannec, Benoit Michel, Guillaume Delamarre, Yves Grohens

Experimental and numerical study of heat transfer across insulation wall of a refrigerated integral panel van

Patrick Glouannec[a,*], Benoit Michel[a], Guillaume Delamarre[a], Yves Grohens[a]

[a]Laboratoire d'Ingénierie des MATériaux de Bretagne (LIMATB), Université de Bretagne-Sud, Université Européenne de Bretagne, Rue de Saint Maudé, BP 92116, 56321 Lorient Cedex, France

Abstract

This paper presents an experimental and numerical design study of an insulation wall for refrigerated vans. The thermophysical properties of the insulating multilayer panel, the external environment impact (solar irradiation, temperature, etc.) and durability are taken into account. Different tools are used to characterize the thermal performances of the insulation walls and the thermal properties of the insulation materials are measured. In addition, an experiment at the wall scale is carried out and a 2D FEM model of heat and mass transfer within the wall is formulated.
Three configurations are studied with this design approach. Multilayer insulation walls containing reflective multi-foil insulation, aerogel and phase change materials (PCM) are tested. Promising results are obtained with these materials, especially the reduction of peak heat transfer and energy consumption during the daytime period. Furthermore, the major influence of solar irradiation is highlighted as it can increase the peak heat transfer crossing the insulation wall by up to 43%. Nevertheless, we showed that the use of reflective multi-foil insulation and aerogel layers allowed decreasing this impact by 27%.

Highlights

A design study of an insulation wall for a refrigerated van is carried out.
Experimental and numerical studies of multilayer insulation walls are performed.
The major influence of solar irradiation is highlighted.
New insulation materials (reflective multi-foil, aerogel and PCM) are tested.

Keywords

Multilayers insulation design, refrigerated vehicle, heat transfer, solar irradiation, instrumentation

*** Corresponding author:**
E-mail: patrick.glouannec@univ-ubs.fr

Nomenclature

c_p	specific heat capacity, $J \cdot kg^{-1} \cdot K^{-1}$	ε	infrared emissivity
e	thickness, m	ΔT	temperature difference, K
E	incident irradiation, $W \cdot m^{-2}$	λ	thermal conductivity, $W \cdot m^{-1} \cdot K^{-1}$
g	gravitational constant, $m^3 \cdot kg^{-1} \cdot s^{-2}$	ρ	density, $kg \cdot m^{-3}$
h	convective heat transfer coefficient, $W \cdot m^{-2} \cdot K^{-1}$	φ	heat flux density, $W \cdot m^{-2}$
K	heat transfer coefficient, $W \cdot m^{-2} \cdot K^{-1}$	Φ	heat flux, W
$\dot{m}$	mass flowrate, $kg \cdot s^{-1}$		
p	pressure, Pa	*Indices*	
T	temperature, K	a	air
u	velocity, $m \cdot s^{-1}$	eq	equivalent
		ext	exterior
Greek symbols		int	interior
α	solar absorptivity	w	wall

1. Introduction

Worldwide, there are about 4 million refrigerated road vehicles, of which about 30% are trailers, 30% large trucks and 40% small trucks and vans (cargo volume below 19 m^3) [1]. It is forecast that by 2030, global road freight transport will have grown by 2.5% a year. Therefore, in order to avoid the increased environmental impact of refrigerated vehicles, it would be of great interest to reduce their energy consumption, especially by improving the insulation design.

The regulations concerning all types of refrigerated vehicles used for the transport of perishable food products require the application of the ATP agreements (Agreement on the International Carriage of Perishable Foodstuffs) drafted by the United Nation in 1970 [2]. According to these standards, insulating performance is characterized by the overall heat transfer coefficient, K ($W \cdot m^{-2} \cdot K^{-1}$), measured in a climatic chamber. Below 0.4 $W \cdot K^{-1} \cdot m^{-2}$, vehicles are classified Reinforced Insulation (IR), while between 0.4 and 0.7 $W \cdot K^{-1} \cdot m^{-2}$ they are classified as normal insulation (IN). These insulation levels are not very ambitious and involve the use of high power chillers.

This experimental K value essentially reflects the vehicle's insulation design (thermal and thermo-optical properties, insulation ageing, vehicle shape, etc.). For example, due to solar irradiation, the thermo-optical properties of the external surface of the vehicle bodywork can account for up to 40% of the energy consumption of the refrigerated unit [3]. In addition, the harsh environmental conditions in a refrigerated vehicle tend to accelerate equipment ageing. Current equipment lifetime is usually between 10 and 15 years for road vehicles [1]. Thus, the thermal performances of the insulation materials deteriorate with time due to migrations of water vapor and expended fluids [4,5]. Several studies have been carried out on the thermal impact of insulation ageing [4,6,7]. In particular, despite a wide experimental data distribution, a typical loss of insulation value of about 5% per year is assumed. It results in a 55% increase of energy consumption and CO_2 emission after nine years.

Furthermore, the manufacturing process can also influence the overall heat transfer coefficient. Estrada-Flores et al. [8] have shown that the K value can vary from 0.82 to 1.24 $W \cdot m^{-2} \cdot K^{-1}$ for similar refrigerated vans.

Thus, it is important to take into account the all these considerations when designing an insulation wall.

Today, the most commonly used insulation material for refrigerated vehicles is expanded polyurethane (PU) foam [5]. It has the advantages of having good mechanical strength, low hydrophilicity and low cost. This material can also be recycled by grinding or chemical treatment but its manufacture requires a great deal of energy. Nevertheless, changes made to the expander agents of PU foam over the past ten years have led to a slight decrease in its insulating capacity [4]. Moreover, the combustion of PU causes the emission of toxic fumes containing hydrogen cyanide (HCN) and isocyanates [9].

The lining is often a polyester (PE) or Acrylonitrile Butadiene Styrene (ABS) composite. This consists in combining a resin (polyester or ABS) with fiberglass (FG) reinforcement to obtain high chemical and mechanical strength. Polyester is generally used for its robustness even at low temperatures. Moreover, it is rot-proof, scratch resistant and easily cleanable. In addition, this polyester skin allows shaping for the vehicle without heavy investment in molds. Nevertheless, the assembly of the panels and the connection between the polyurethane and the polyester skin is done by bonding which does not allow optimized recycling. Thus the design is far from being perfect from the environmental point of view.

New insulation materials have appeared on the market and seem to be good candidates for improving the insulation of refrigerated walls (aerogels, phase change materials (PCM), etc.). These materials have been widely studied for building insulation [9,10] and for cold storage applications [11,12]. In contrast, insulation applications for refrigerated vehicles have not been studied extensively. Nevertheless, a recent study [14] has shown that, in Europe, the use of PCM in refrigerated vehicles could reduce energy consumption from 959 to 12,788 GWh/y. Moreover, promising results have been obtained by integrating PCM in the insulation walls of refrigerated vehicles. Thus, Ahmed et al. [14] carried out an experimental study of PCM inclusion in a standard refrigerated trailer wall. Copper pipes were filled with paraffin-based PCM and integrated in a PU insulation wall. The experiment performed with a small-scale refrigerated trailer resulted in an average reduction of peak heat transfer

of 29.1% and an average energy saving of 16.3%, compared to a standard refrigerated trailer. Furthermore, Tinti et al. [15] studied the design of a PU foam insulation wall containing 4.5% to 13.5% in weight of a micro-encapsulated PCM. The thermographic analysis of these composites irradiated by a directional heat source showed that the higher the PCM content within the PU foam was, the lower the heat flow transmitted by the specimen.
In addition, refrigerated trailer insulation walls can be improved by using multilayer composites whose insulation characteristics can be improved by thermal radiation protection.

This paper focus on the insulation walls of a van fully equipped with refrigerated panels (vehicle with insulation and refrigeration equipment added to the basic shell). This kind of vehicle is usually used to transport refrigerated products over a period of a few hours (meal trays, medical products, etc.). The objective is to present an insulation wall design approach that takes into account the thermal properties of the insulating multilayer panel, the impact of the external environment (solar radiation, temperature, etc.), durability and recyclability.
The paper presents an experimental and numerical study of an insulation wall for a refrigerated panel van. The first part is dedicated to the experimental and numerical tools set up to characterize the transient thermal response of different wall configurations. Thus a wall scale experiment and a 2D model of heat and mass transfer within the insulation wall are implemented and described. In parallel, methods for characterizing the thermal properties of insulation materials are defined. A detailed study of the different wall configurations is presented in the second part.

2. Materials and method

2.1. Multilayer insulation walls

2.1.1. Experimental set-up

An experiment was carried out to characterize the heat transfer through a 0.86 m^2 wall. Figure 1a shows the "reference" configuration. From the inside to the outside it consisted of an insulating multilayer panel, an air gap of 10 cm and, finally, the bodywork of the vehicle (sheet metal 0.1 cm thick). The insulating multilayer panel was composed of 5.8 cm of polyurethane foam, to which was glued an inner skin of polyester and fiberglass composite (0.2 cm) and an outer skin of fiberglass (0.1 cm). The thickness of the layer of skin glue was about 0.1 cm.
One side of the insulation wall was placed in an insulated enclosure with a volume of 0.5 m^3 (Figure 1b), whose interior temperature (Tint) was controlled by an air conditioning system designed to blow air at temperatures from 0°C to 70°C (with an uncertainty of ± 2°C). The whole assembly was placed in a climatic chamber designed for use over a temperature range from -20°C to 50°C. This configuration therefore made it possible to simulate the temperature conditions both inside and outside a refrigerated vehicle.

To observe the thermal response of the walls tested, a full array of instruments was installed. Several K type thermocouples were located at different positions (Figure 1b). Thus the temperatures of the inner side of the bodywork (T1), the middle of the air gap (T2), the outer and inner side of the insulating multilayer panel (T3 and T5) and the inside of the PU (T4) were measured at the mid-height of the wall. Additional thermocouples were placed on the top and the bottom part of the wall: for the inner side of the bodywork, the air gap and the outer side of the insulation multilayer panel. Moreover, two thermocouples were used to measure the temperatures of the climatic chamber (T_{ext}) and the internal insulation box (T_{int}).
In order to measure the heat flux density crossing the wall, a heat fluxmeter of 5cm x 5cm (Captec) was glued on the inner face of the multilayer insulation panel, at mid-height. The thickness of the heat flux meter was 0.4 mm and its sensitivity 7.5 $\mu V/W/m^2$.
Moreover, punctual measures of the air velocity on each side of the wall were carried out with an omnidirectional hot-wire anemometer.
Finally, for several experiments two sunlamps (Honle UVASPOT 1200) were placed in front of the bodywork in order to reproduce the sunlight. To quantify the average incident solar irradiation, the

wall surface was discretized into twelve parts and solar irradiation was measured punctually with a pyranometer (Kipp & Zonen, CMP 11).

All the sensors were connected to a Keithley 2701 data logger. The evaluation of the uncertainties on the sensors and the measurement chain is summarized in Table 1.

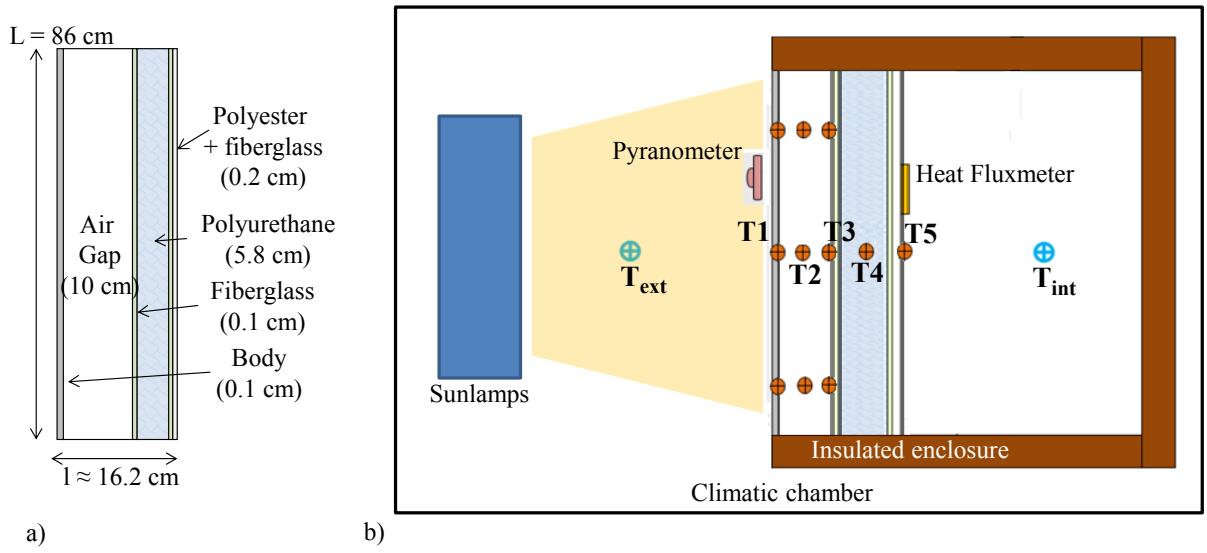

Figure 1: Schematic overview a) of the insulation wall and b) of the experimental bench.

Sensor	Accuracy
Heat fluxmeter	±5%
Thermocouple type K	±0.5°C
Pyranometer	±3%
Anemometer	±0.1 $m \cdot s^{-1}$

Table 1: Sensors and evaluation of their measure uncertainties.

2.1.2. Numerical model

In parallel with the experimental characterization, a 2D dynamic FEM model, coupling heat and mass transfer within the insulation wall, was built. This model, solved with commercial software (COMSOL®), permitted the detailed analysis of the heat transfers within the wall.
Each layer of the insulating wall and thermal boundaries was taken into account but the presence of adhesive layers in the insulation multilayer panel (thickness about 0.1 cm) was omitted. Moreover, we assumed that the top and bottom of the wall (faces (5) and (6) in Figure 2) were adiabatic. The phenomena involved and the geometry modeled are shown schematically in Figure 2. The set of equations required by this model is described below.

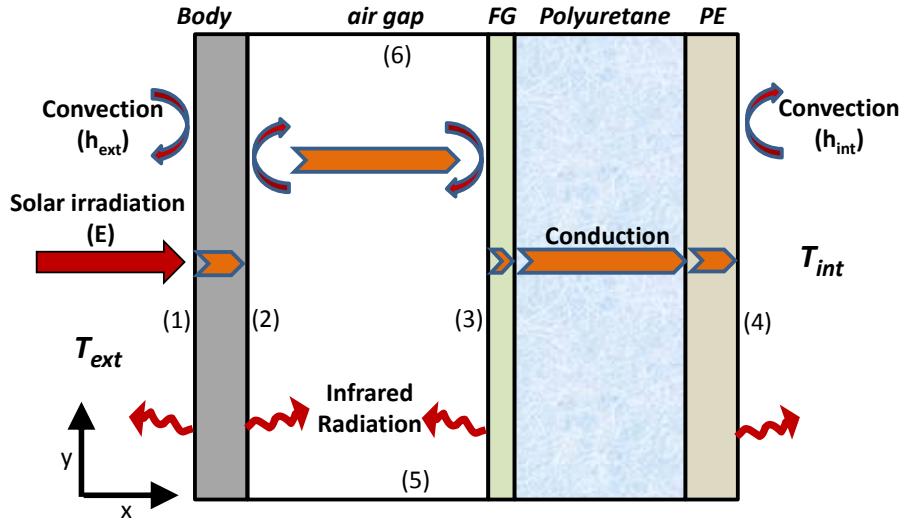

Figure 2: Schematic representation of the insulating wall (numbers refer to boundary conditions described below).

a) Energy and mass balance

The air gap is assumed perfectly transparent and only the surface to surface radiation is taken into account. Moreover, the heat transfer is conductive according to Fourier's law and convective, thus the energy balance is given by the following equation, coupled with the mass balance equation [16]:

$$\rho c_p \frac{\partial T}{\partial t} + \rho c_p \vec{u} \cdot \nabla \mathrm{T} = \nabla \cdot (\lambda \nabla T) \quad (1)$$

Moreover, the air gap is considered as an incompressible Newtonian fluid, thus a Navier-Stokes equation is used:

$$\rho \left[\frac{\partial \vec{u}}{\partial t} + (\vec{u} \cdot \nabla) \cdot \vec{u} \right] = -\nabla p + \mu \Delta \vec{u} - \rho \vec{g} \quad (2)$$

Finally, in the solid layers the heat transfer is only conductive. The energy balance can be written as:

$$\rho c_p \frac{\partial T}{\partial t} = \nabla \cdot (\lambda(T) \nabla T) \quad (3)$$

The resolution of this system of equations with the finite element method allows obtaining the thermal response of the insulating wall as a function of the initial and boundary conditions described in the following paragraph.

b) Boundary conditions

- Face (1): external wall-side of the vehicle

Convective and infrared radiative heat fluxes are taken into account between the face and the outside environment. Moreover, an incident solar irradiation, E, can be imposed. Thus, we have:

$$-\lambda \nabla T = \varepsilon \sigma (T_{ext}^4 - T^4) + h_{ext}(T_{ext} - T) + \alpha E \quad (4)$$

- Face (2) and (3): air gap walls

A conductive heat flux and a surface to surface radiative heat flux between each face are imposed:

$$\lambda_w \nabla T_w = \lambda_a \nabla T_a + \varepsilon (G - \sigma T_w^4), \quad (5)$$

with G being the incident radiative heat flux coming from the other boundaries.
Moreover, the normal velocity at the boundary is null:

$$\frac{\partial u_x}{\partial x} = 0, \quad (6)$$

- Face (4): internal wall side

Convective and radiative heat fluxes are taken into account:

$$-\lambda\nabla T = \varepsilon\sigma\left(T^4 - T_{int}^4\right) + h_{int}(T - T_{int}), \quad (7)$$

The outside and inside convective coefficients, $h_{ext/int}$, are determined from measures of air velocities and using standard correlations for convective coefficients along a flat plane [17].
Initially, uniform temperature is imposed at the insulating wall and the air velocity in the air gap is set to zero.

2.2. Characterization of the material properties

In order to simulate the thermal response of the walls, the thermo-physical and thermo-optical properties were measured.

The solar absorptivity is determined using a UV spectrometer (Shimadzu UV 3600) equipped with a 15 cm diameter integrating sphere. The spectral band covered by the device ranged from 300 to 2,400 nm, which covered 93% of incoming solar irradiation. For the infrared emissivity a spectrometer (Vertex 70) equipped with a 15 cm diameter integrating sphere was used. The spectral band covered by the device ranged from 710 to 25,000 nm.

The heat capacity was measured on the thermal range -5 to 40°C, with a differential scanning calorimeter (MDSC3-SETARAM) and the density at ambient temperature by pycnometry. The uncertainty on the measurement of the volumetric thermal capacity was 5%.
In accordance with standard ISO 8301, the thermal conductivity of each material was determined with a conductivimeter (NETZSCH HFM 436/3) in the temperature range from 0 to 50°C.
This apparatus was also used to measure the equivalent heat transfer coefficient, K_{panel}, of the insulating multilayer panel samples having a surface area of 30cm×30cm and variable thickness:

$$K_{panel} = \frac{\varphi}{\Delta T} \quad (8)$$

with φ the heat flux densities and ΔT the temperature difference.
The uncertainty was evaluated at 5%.

In order to complete the characterization of the multilayer insulation, experiments were performed to quantify insulation ageing effects. The equivalent heat transfer coefficient was measured before and after an ageing procedure. The method of accelerated aging under moist heat was used for the test. This method corresponds to standard PSA D47 1165, used to carry out the accelerated ageing of a vehicle wall. Its consists in surrounding the sample with wet cotton wool, placing it in a sealed polyethylene bag and then aging the sample for 60 days in a climatic chamber at high temperature (10 days at 50°C, then 10 days at 70°C and, finally, 40 days at 50°C). Moreover, at the end of the ageing test, before the measurement of the heat transfer coefficient, the sample without the wet cotton wool is placed for one day in an oven at 70°C.

3. Results and discussion

In the first part, the performances of the reference wall (Figure 1) are described and studied. In the second part, two other configurations (Figure 6) built to improve thermal performances are presented. Finally, the influence of solar irradiation on the thermal response is analyzed.
The thermal conductivities of the materials of the different walls presented in this part are summarized in Table 2.

	PU	PE + Fiberglass	Fiberglass	RMF	Aerogel	Energain	Bodywork (sheet metal)
λ (W·m^{-1}·K^{-1})	0.022	0.64	2	0.035	0.0217	0.18 Solid 0.14 Liquid	60

Table 2: Thermal conductivities of the different materials at 15°C.

3.1. Reference case

3.1.1. Equivalent heat transfer coefficient of a multilayer sample

Firstly the equivalent heat transfer coefficient and the ageing study of the reference insulation multilayer panel are presented. We recall that this multilayer panel was composed of an insulation layer of polyurethane foam and a lining of polyester and fiberglass (Figure 1a).

Figure 3 gives the values of the heat transfer coefficient as function of temperature, before and after the ageing test (sixty days). Before the ageing test, an equivalent heat transfer coefficient of 0.40±0.04 $W \cdot m^{-2} \cdot K^{-1}$ at 15°C was obtained.

After sixty days ageing, an increase of the heat transfer coefficient was observed for a temperature above 30°C. Thus, at 50 °C, the heat transfer coefficient increased by 11%. This phenomenon was certainly due to the migration of water vapor into the PU. Furthermore, the literature indicates that the migration of gas emitted by the PU and the migration of the outside air into the PU [4,18] can also lead to an increase of thermal conductivity. Moreover, no significant evolution of the heat transfer coefficient was observed below 30°C.

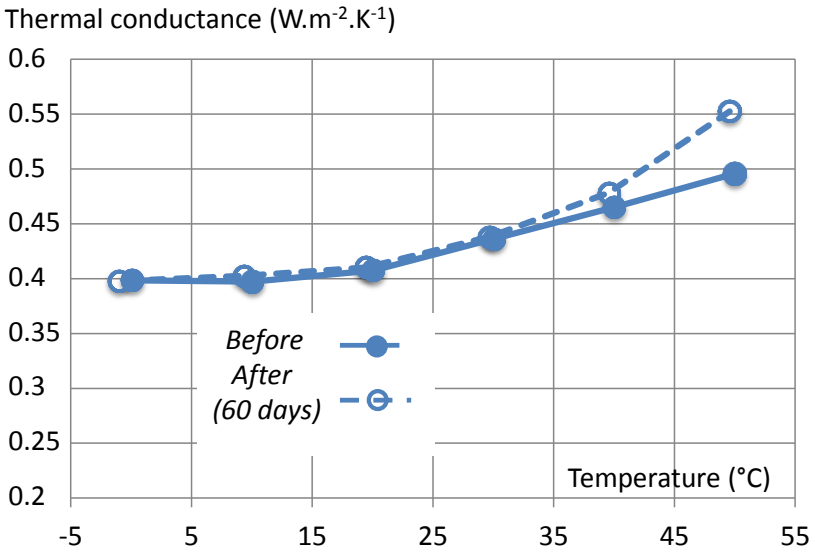

Figure 3: heat transfer coefficient as function of temperature for the reference insulation multilayer panel (PE+PU), before and after 60 days of ageing test.

3.1.2. Experimental and numerical study of the wall

In order to replicate a standard use scenario of a refrigerated panel van which transports goods over a period of several hours, the following experimental protocol was used for the tests.

We assume that the refrigerated transport van was subjected to cold temperature at night and then performed a delivery round (daytime). The initial temperature of the wall was 20°C. That of the environment, T_{ext}, was then set at 10°C for four hours and then at 30°C (environment temperature during a summer delivery round) for the last hours. During the eight hours of the experiment, the internal temperature, T_{int}, was maintained at 0°C (set point cooling temperature).

Figures 4a & Figure 5 show the experimental and simulated results for the temperature and heat flux density (Figure 1). The convective exchange values used in the simulation were h_{int}=3 and h_{ext}=7 $W \cdot m^{-2} \cdot K^{-1}$. The measures of air velocity near the outside and inside surface of the wall were respectively around 1.2 $m \cdot s^{-1}$ and 0.5 $m \cdot s^{-1}$.

In addition, the temperature profile in the insulation wall at the 7th hour is presented in Figure 4b.

First of all, we observe that in steady-state, the external temperature was slightly lower, about 1°C, than the set temperature (10°C during the “nighttime period” and 30°C during the “daytime period”).

However, the internal temperature was close to 0°C, despite some oscillations, especially at the beginning of the experiment, due to the regulation of the refrigeration unit.
The start of the experiment was characterized by a quick fall in the wall temperatures, by about 10°C in a few minutes. This led to a peak heat flux. Then, between the 2nd and 4th hours and the 6th and 8th hours, two steady state periods were observed. These periods corresponded to the nighttime and daytime periods, of the refrigeration vehicle protocol.
As is logical, it can be seen that the temperature gradient is highest in the polyurethane (between T3 and T5), which fulfills its role of insulation (Figure 4b). On the contrary, the temperature gradient remained low within the air gap (between T1 and T3), due to substantial infrared radiative and convective exchanges. Note that the air gap temperature, T2, which is only presented at the seventh hour (Figure 4b), is between T1 and T3 throughout the experiment.

The air gap temperature measures show that the vertical temperature gradient is low (not presented). Indeed, during the steady state of the delivery round period (from the 6th to 8th h), the temperature gradient between the top and the bottom of the wall was less than 1°C. Thus, the temperature and the heat flux density profiles at the center of the wall can be considered as representative of the thermal phenomena of the whole wall. Consequently, only data from the mid-height of the wall are presented in this paper.

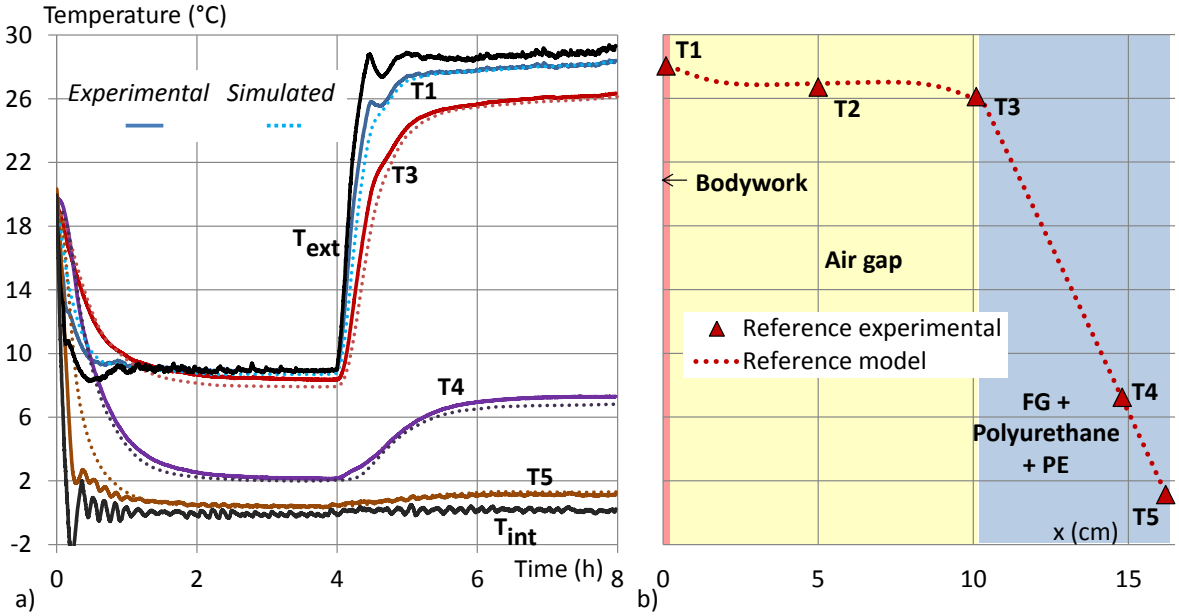

Figure 4 : Experimental and simulated wall temperature profiles of the reference case a) as function of time, b) inside the insulating wall, at t=7h.

Figure 5 shows that in steady-state, the heat flux density reaches about 10.4 W.m^{-2} for a difference in temperature of 24.2 °C between the inner and outer sides of the multilayer insulation panel. Thus, the equivalent heat transfer coefficient of 0.42±0.04 W·m^{-2}·K^{-1} (eq.8) is obtained. This value is close to the measures of the conductivimeter (K_{panel}=0.40±0.04 W·m^{-2}·K^{-1} at 15°C).

This experiment also allowed determining the global heat transfer coefficient of the wall (K_{wall}) from the air temperature (T_{int} and T_{ext}). A value of 0.39±0.03 W·m^{-2}·K^{-1} was obtained. This value is at the limit of the reinforced insulation of the ATP classification, but it is considerably lower than the overall heat transfer coefficient of refrigerated vans identified by Estrada-Flores et al. [8] (from 0.82 to 1.24 W·m^{-2}·K^{-1}).

Furthermore, the energy required to maintain the temperature low inside the refrigerated enclosure during the daytime period (4th to 8th hour) was 117±6 J/m^2. All of these results are summarized in Table 3.

	Reference case	Case 1	Case 2
K_{panel} (W/m²/K)	0.42±0.04	0.33±0.03	-
K_{wall} (W/m²/K)	0.39±0.03	0.24±0.02	-
Energy consumption during the day time period (kJ/m²)	117±6	83±4	88±4

Table 3: Multilayer panel (K_{panel}) and wall (K_{wall}) heat transfer coefficient of the reference case, case 1 and case 2 as well as their energy required to keep low temperature inside the refrigerated enclosure per wall surface unit, during the daytime period (4th to 8th hour).

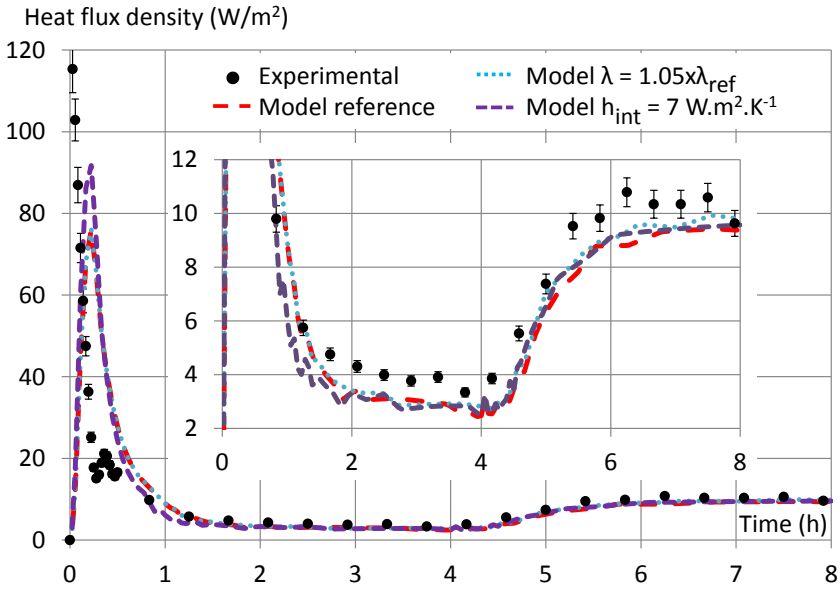

Figure 5: Heat flux densities at the inner side of the insulating wall as function of time, for the reference case.

Finally, the simulation results are close to the experimental data (Figure 4 and Figure 5). Indeed, the model predicts the temperature profile well during the steady state periods. Between the 6th and the 8th hour, the average deviation of T5 is less than 7% and the deviation of T1 is about 0.1%. During transient periods (first two hours and between the 4th and the 6th hour), the temperature trends are well represented. However, it can be seen that the simulated temperature (T5) of the inner insulating surface is overestimated during these periods. This may be due in part to an underestimated internal convection coefficient (h_{int}) determined from the measured internal air velocities (§2.2).

The heat flux density trends were also well predicted by the model, although they were slightly underestimated (by about 12% during steady-state periods and at most 36% during the peak occurring at the start of the experiment). One explanation for this gap may be the uncertainties on the measurements of the heat flux density and the thermal properties of the materials (Table 1).

A parametric study was carried out. Figure 5 presents the influence of two parameters: the inside convective coefficients, h_{int}, and the thermal conductivity of the PU. Thus, increasing the thermal conductivity of the PU by 5% led to an increase of heat transfer during the steady-state period (of 4.2% between the 6th and 7th h). On the contrary, the inside convective coefficient mainly influenced the transient periods. Thus, increasing h_{int} from 3 to 7 $W \cdot m^{-2} \cdot K^{-1}$ allowed increasing the simulated heat flux peak by 23%.

Admittedly, the simulated results were sensitive to the input model parameters. Therefore, taking into account the uncertainties, we observe that the predictions of the model were acceptable throughout the test.

3.2. New wall configurations

In order to validate the experimental methodology presented previously and to increase the insulation performances, two different wall configurations were studied. These configurations corresponded to the addition of thin layers of new materials at the reference wall which did not penalize the mass and the useful volume of the vehicle (Figure 6).

In case 1, an insulating layer of 1 cm of aerogel (Pyrogel XT®) and one layer of reflective multi-foil insulation (RMF) were placed on the inner side of the air gap (Figure 6a). Note that the aerogel and the RMF layers were not glued as this could lead to additional thermal resistance.

Another wall configuration incorporating a layer of PCM (Energain®) was tested (case 2). The aim of this layer was to limit refrigerating demand during the daytime period and thus decrease the refrigerating power and energy requirement. To do this, the refrigerating demand was shifted from the daytime period to the nighttime period. Thus, a layer of Energain® 0.5cm thick was placed on the outside of the multilayer insulation panel (Figure 6b). As with the aerogel and RMF layers, the PCM layer was not glued to the multilayer insulation panel.

The Energain® panels, manufactured by Dupont de Nemours [19], are composed of 60% paraffin microencapsulated within a copolymer. These panels are usually used in building construction, especially in interior walls or ceilings, for thermal energy storage. Its melting and freezing kinetics were measured using the DSC method (§2.2), with a temperature variation rate of 0.2 K/min. The melting temperature and phase change enthalpy deduced in the temperature range 5-30°C were 21°C and 72.9 $J.g^{-1}$. Similarly, its freezing temperature and latent heat were 16°C and 75.7 $J.g^{-1}$. We noted a difference between the melting and freezing temperatures. This hysteresis effect of PCM is well-known and is intrinsic to the material [20]. Similar enthalpy values are presented in the literature. However peak of melting and freezing temperatures of 17.8 and 22.3°C have been highlighted [21].

Therefore, on the basis of the temperature profiles of the reference case (Figure 4), and in order to allow melting during daytime and freezing during nighttime, the Energain layer was placed on the outer side of the multilayer insulating panel (Figure 6b).

The thermal conductivities of these materials are summarized in Table 2.

Finally, for both the new configurations, thermocouples were added on the outside multilayer insulation panel. Thus T3' and T3'' were respectively added for case 1 and case 2.

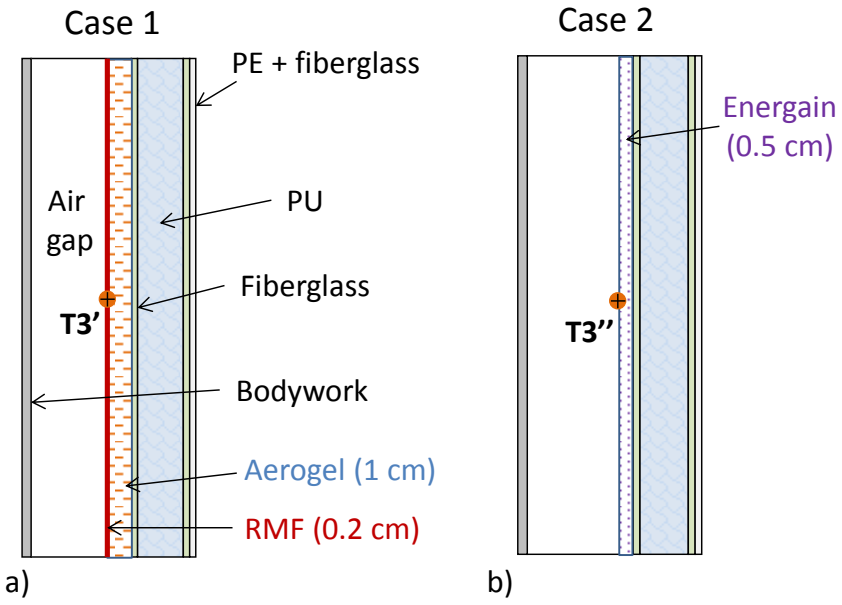

Figure 6: Schematic overview of the insulation walls: a) case 1 and b) case 2.

3.2.1. Aerogel+RMF

Figure 7a presents the heat flux density as a function of time for the different multilayer walls. As

expected, during the daytime period (4th to 8th h) the thermal losses of case 1 are significantly lower than for the reference case. Thus, the energy consumption is 83±4 J·m^{-2} during this period, corresponding to a gain of 36% (Table 3). The corresponding heat transfer coefficient of the multilayer panel and the wall are 0.33±0.03 and 0.24±0.02 W·m^{-2}·K^{-1}.

The experimental and simulated wall temperature profiles at the 7th hour are presented in Figure 7b. First, it can be seen that the simulated temperatures are consistent with the experimental results for both cases. Then, that the RMF+aerogel layer considerably decreases the temperature of the multilayer insulation panel and therefore fulfills its role of insulation. Thus the temperature of the outer face of the PU (T3) decreases by 9.4°C for case 1 compared to the reference wall. Moreover, the temperature of the outer side of the multilayer insulation panel is lower for case 1 (T3'=21°C) than for the reference case (T3=26°C). This phenomenon shows that the RMF layer is an interesting insulation solution.

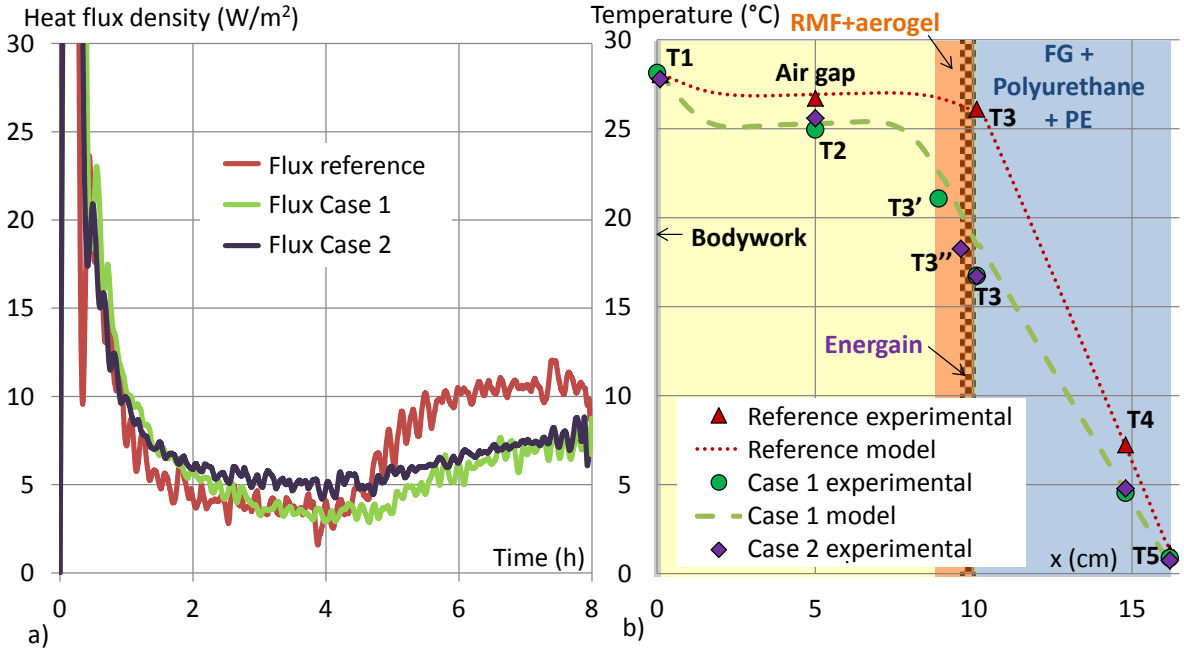

Figure 7: Results for the reference case and the cases 1 and 2:
a) experimental heat flux densities at the inner side of the insulating wall as function of time,
b) experimental and simulated temperatures within the insulating wall, at t=7h.

3.2.2. Phase change material: Energain

Figure 7a shows that during the four first hours of the experiment (nighttime period), the heat flux density of case 2 is equivalent or slightly higher than the reference case, although the multilayer panel insulation thickness is slightly higher. This is due to the cold storage in the PCM. Therefore, these four hours are insufficient to charge completely the PCM layer.

However, the heat flux variation between nighttime and daytime periods is lower when PCM is integrated in the insulation wall. Indeed, between the 4th and the 6th hour, the heat flux density increases by 7.5 W.m^{-2} for the reference case and by only 3.2 W.m^{-2} for the wall with PCM. Globally, during the daytime period, the energy consumption decreases by about 25% compared to the reference case (Table 3). Thus, the PCM layer fulfills its role of cold storage between the nighttime and daytime periods.

Moreover, Figure 7b shows that during the daytime period (at the 7th h) the temperature profile of case 2 is similar to that of case 1. Thus, compared to the reference case, we observed a significant decrease in the temperature of the outer side multilayer due to the melting of the Energain® layer.

To better understand functioning of the PCM wall, a longer experiment with configuration 2 (eight hours nighttime period and eight hours daytime period) was carried out. The heat flux density and temperatures within the insulation wall are presented in Figure 8. We remark that steady-state was not reached during either the nighttime period or the daytime period. Indeed, the temperatures and the heat flux density were not stabilized. Moreover, at the end of the experiment the PCM layer boundary temperatures (T3'' and T3) were close to the Energain® melting temperature (21°C). This shows a partial melting of the PCM.

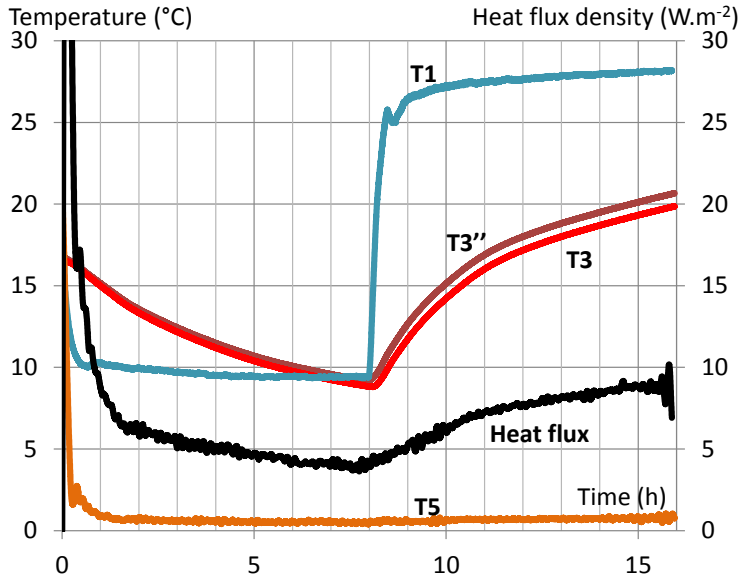

Figure 8: Configuration 2 during a long experimentation: experimental temperatures and heat flux as function of time.

3.3. Tests with solar irradiation

Further tests and simulations subjecting the outer wall side (bodywork) to solar irradiation were carried out. Thus, a study of the impact of solar irradiation on the reference case and case 1 is presented below.
Constant solar irradiation of 460 W·m^{-2} was applied from the 4th to the 6th hour to the outside surface of the wall. Except for the solar irradiation, the test protocol was similar to that of the previous experiment described in §3.1.2.

Figure 9a shows the heat flux densities measured and simulated for case 1 and the reference wall. As can be seen, the influence of solar irradiation is significant. This effect is largest for the reference case (without RMF). Indeed, compared to the experiments without solar irradiation, the heat flux density peak increases by 43% (from 10.5 to 15 W·m^{-2}) for the reference case, while it increases by 31% for case 1 (from 8 to 10.5 W·m^{-2}), corresponding to a decrease of 27% compared to the reference case. Thus the aerogel and RMF layers limited the increase of heat flux due to solar irradiance.
By comparison, in the literature [15] a study of a refrigerated box insulated using a conventional method for refrigerated trailers showed an increase of 180% of the heat transfer peak, between the north face (without solar irradiation) and the south face (with solar irradiation) of the box, for a peak solar irradiation of 550 W·m^{-2}. The better performances of the walls studied in this paper could be due to the air gap, which allowed reducing the impact of solar irradiation. Indeed, Figure 9b presents the experimental and simulated temperature profiles of case 1. We note that the peak air gap temperature (T2) during the irradiation period is about 10°C lower than the peak bodywork temperature (T1).

Furthermore, although the irradiation period leads to a strong increase of the bodywork (T1) and air gap (T2) temperatures (respectively about 20°C and 15°C, compared to the steady-state temperature of case 1 without solar irradiation (Figure 7)). The increase of the outer insulation multilayer panel temperature (T3) is only of 8°C. This highlights RMF interest to reduce the solar irradiation impact.

Finally, Figure 9 shows that the simulated temperatures are close to the experimental results. Moreover, although the heat flux density during the "nighttime period" is slightly underestimated, good consistency between the experiment and the simulation can be seen for case 1. Therefore, the 2D model predicts the local and global performances of the wall correctly, with and without solar irradiation.

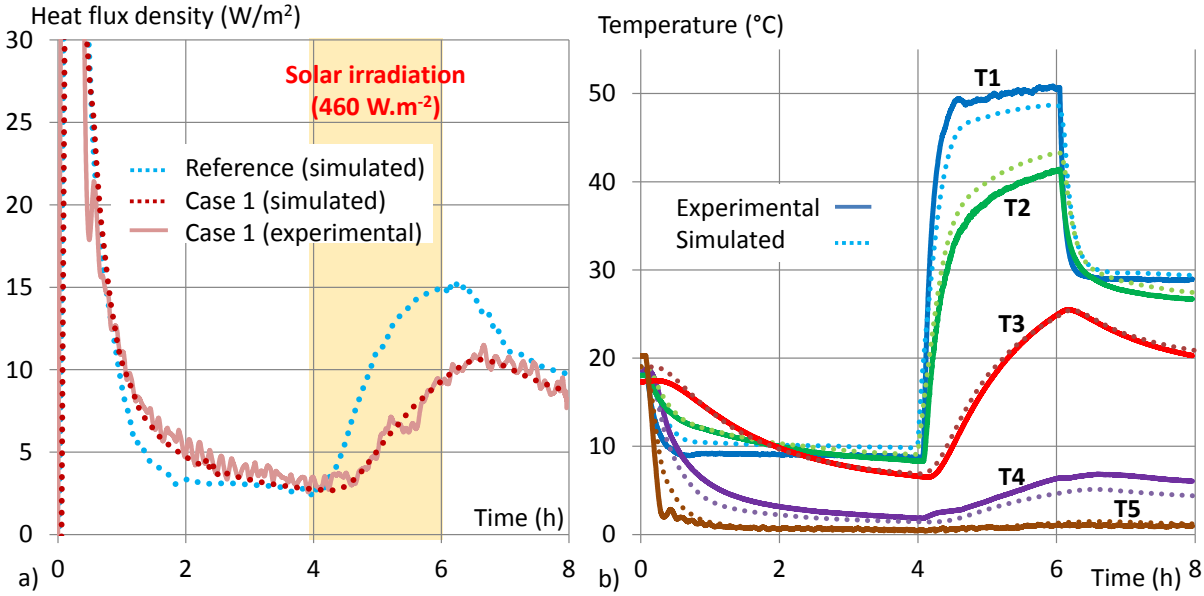

Figure 9: a) Heat flux densities at the inner side of the wall as function of time, for the reference case (simulated) and the case 1 (experimental and simulated), with solar irradiation
b) Experimental and simulated wall temperatures for the case 1 with solar irradiation.

4. Conclusion

This paper presented an experimental and numerical design study of an insulation wall for refrigerated integral panel van, taking into account the thermal properties of the insulating multilayer panel, the impact of the external environment (solar irradiation, temperature) and durability.

The different experimental and numerical tools developed allowed the dynamic characterization of the thermal transfer within several multilayer insulation walls. The interest of increasing the wall insulation was highlighted. In particular, reflective multi-foil insulation and aerogel layers gave good results, especially for limiting peak heat transfer and energy consumption during the daytime period. Thus, increasing the multilayer panel thickness by 20% led to a 36% reduction of energy compared to a reference case.

Promising results were also obtained with the increase of wall inertia using a PCM layer (Energain®). Nevertheless, for the experimental conditions tested, the Energain® layer could not fully melt or freeze during the eight-hour experimental periods. Work to optimize the size, emplacement and choice of the PCM layer are underway to increase the performances of the insulation wall.

Moreover, this study showed that the evaluation of the wall heat transfer coefficient according to the ATP criteria is insufficient. Thus the considerable influence of solar irradiation was highlighted. This can increase the peak heat transfer by up to 43%. However, we showed that this effect can be reduced by 27% using an aerogel + RMF layer.

In parallel, the ageing of the insulation multilayer panel was taken into account. For the reference wall, an average decrease of the thermal performance of 3% was obtained with a specific ageing experiment.

Acknowledgments

We thank the Bpifrance and the Brittany region for their financial support of the ISO4CAR project, labeled by the ID4CAR cluster. We also thank the GRUAU company which was responsible for coordinating the project.

References

[1] UNEP/Earthprint, Report of the Refrigeration, Air Conditioning, and Heat Pumps Technical Options Committee, 2010.
[2] UNECE Transport Division, United Nations. Agreement on the international carriage of perishable foodstuffs and on the special equipment to be used for such carriage (ATP), Geneva, Switzerland, 1970.
[3] G. Cavalier, 26 challenges facing refrigerated trucks for sustainable development, Ind. Formazione. supp 1 (2010).
[4] G. Panozzo, G. Minotto, A. Barizza, Transport et distribution de produits alimentaires: situation actuelle et tendances futures, Int. J. Refrig. 22 (1999) 625–639. doi:10.1016/S0140-7007(99)00023-7.
[5] S.A. Tassou, G. De-Lille, Y.T. Ge, Food transport refrigeration – Approaches to reduce energy consumption and environmental impacts of road transport, Appl. Therm. Eng. 29 (2009) 1467–1477. doi:10.1016/j.applthermaleng.2008.06.027.
[6] S.K. Chatzidakis, K.S. Chatzidakis, Refrigerated transport and environment, Int. J. Energy Res. 28 (2004) 887–897. doi:10.1002/er.1002.
[7] TRANS/WP.11/2000/9, Economic Commission for Europe, Inland Transport Committee, Working Party on the Transport of Perishable Foodstuffs, Economic Commission for Europe, Inland Transport Committee, Working Party on the Transport of Perishable Foodstuffs, Geneva, Switzerland, 2000.
[8] S. Estrada-Flores, A. Eddy, Thermal performance indicators for refrigerated road vehicles, Int. J. Refrig. 29 (2006) 889–898. doi:10.1016/j.ijrefrig.2006.01.012.
[9] B.P. Jelle, Traditional, state-of-the-art and future thermal building insulation materials and solutions – Properties, requirements and possibilities, Energy Build. 43 (2011) 2549–2563. doi:10.1016/j.enbuild.2011.05.015.
[10] B. Zalba, J.M. Marín, L.F. Cabeza, H. Mehling, Review on thermal energy storage with phase change: materials, heat transfer analysis and applications, Appl. Therm. Eng. 23 (2003) 251–283. doi:10.1016/S1359-4311(02)00192-8.
[11] E. Oró, A. de Gracia, A. Castell, M.M. Farid, L.F. Cabeza, Review on phase change materials (PCMs) for cold thermal energy storage applications, Appl. Energy. 99 (2012) 513–533. doi:10.1016/j.apenergy.2012.03.058.
[12] E. Oró, L.F. Cabeza, M.M. Farid, Experimental and numerical analysis of a chilly bin incorporating phase change material, Appl. Therm. Eng. 58 (2013) 61–67. doi:10.1016/j.applthermaleng.2013.04.014.
[13] E. Oró, L. Miró, M.M. Farid, V. Martin, L.F. Cabeza, Energy management and CO2 mitigation using phase change materials (PCM) for thermal energy storage (TES) in cold storage and transport, Int. J. Refrig. (2014). doi:10.1016/j.ijrefrig.2014.03.002.
[14] M. Ahmed, O. Meade, M.A. Medina, Reducing heat transfer across the insulated walls of refrigerated truck trailers by the application of phase change materials, Energy Convers. Manag. 51 (2010) 383–392. doi:10.1016/j.enconman.2009.09.003.
[15] A. Tinti, A. Tarzia, A. Passaro, R. Angiuli, Thermographic analysis of polyurethane foams integrated with phase change materials designed for dynamic thermal insulation in refrigerated transport, Appl. Therm. Eng. (2014). doi:10.1016/j.applthermaleng.2014.05.003.
[16] F.P. Incropera, D. Dewitt, T. Bergman, A. Lavine, Fundamentals of heat and mass transfer., John Wiley, Hoboken, NJ, 2007.
[17] M.N. Özışık, Heat transfer: a basic approach, McGraw-Hill, 1985.
[18] J. Evans, Frozen Food Science and Technology, John Wiley & Sons, 2009.

[19] The Homepage of Energain®, DuPont Glob. Website. http://energain.co.uk (2014).
[20] H. Mehling, L.F. Cabeza, Heat and cold storage with PCM: An up to date introduction into basics and applications, Springer, 2008.
[21] F. Kuznik, D. David, K. Johannes, J.-J. Roux, A review on phase change materials integrated in building walls, Renew. Sustain. Energy Rev. 15 (2011) 379–391. doi:10.1016/j.rser.2010.08.019.